Capturing Small Asteroids into a Sun-Earth Lagrangian Point

Neus Lladó[a,*], Yuan Ren[b], Josep J. Masdemont[c], Gerard Gómez[d]

[a] *Elecnor Deimos, Spain*
[b] *Department of Earth and Space Science and Engineering, York University, Canada*
[c] *IEEC & Departament de Matemàtica Aplicada I, Universitat Politècnica de Catalunya, Spain*
[d] *IEEC & Departament de Matemàtica Aplicada i Anàlisi, Universitat de Barcelona, Spain*

Abstract

In this paper we address the feasibility of capturing small Near-Earth Asteroids (NEAs) into the vicinity of the Sun-Earth L_2 libration point using a continuous-thrust propulsion system assumed attached to the asteroid. The vicinity of this libration point is a gateway to the Earth-Moon neighborhood and using it for capture, or for transit, small NEAs could be interesting for mining or science purposes.

Due to limited maneuver capabilities and security concerns, only NEAs with very small mass, and not representing a potential hazard, are analyzed. First, the NEAs are pruned from JPL NEAs [1] database and their diameter and mass are estimated using two different methods based on physical properties. Then, fuel-optimal continuous-thrust transfer orbits from the original positions of the NEAs to the Sun-Earth L_2 libration point are computed. For this trajectory optimization, the initial seeds are generated by means of a global optimization procedure based on a differential evolution algorithm. Next, these initial seeds are refined with a fourth order Runge-Kutta shooting method, and finally we list the candidate NEAs to be captured using a continuous-thrust propulsion system including the key parameters defining their transfer trajectory.

Keywords: asteroid mining, libration point, continuous-thrust, trajectory optimization

*Corresponding author
Email addresses: neus.llado@elecnor-deimos.com (Neus Lladó), yren@yorku.ca (Yuan Ren), josep@barquins.upc.edu (Josep J. Masdemont), gerard@maia.ub.es (Gerard Gómez)

1. Introduction

The asteroid mining concept considers the exploitation of raw materials from asteroids and other minor planets [2]. Raw materials could be used in space for construction, rocket propellant or they could be taken back to the Earth. The asteroid mining technology is believed to play an important role in providing resources for future Solar System exploration missions and it may also provide key elements needed in modern industry. According to [3], antimony, zinc, tin, silver, lead, indium, gold, and copper could be exhausted on Earth within $50 - 60$ years.

A rough spectral taxonomy of asteroid types divides them in three main groups: C-group (carbonaceous), S-group (stony) and X-group (mostly metallic). The Near Earth Asteroids group C are the objects that could be the easiest to be exploited for raw materials. In this paper we investigate the possibility of exploiting the materials on the NEAs from the point of view of space-dynamics. From a mechanic and robotics point of view, attending also the fact to un-spin the asteroid, that is not much expensive, we refer to [4, 5].

Different from the standard concept of asteroid mining, we use a novel mining strategy. Instead of mining on the original orbit of the NEA and take the raw materials back to the Earth, we consider to capture the NEA into the Sun-Earth L_2 vicinity by means of a continuous-thrust propulsion system [6, 7, 8]. This strategy has two advantages. If we exploit a NEA on its original orbit, only if the relative phase between the Earth and the NEA is the suitable one, the mining robot can be sent to the NEA and the raw materials can be sent back to the Earth. If a NEA is captured into the Sun-Earth L_2 vicinity, the transport between the Earth and the NEA no longer has this limitation. Second, the Sun-Earth L_2 point is a saddle point from the dynamical point of view. The NEA can be temporarily captured in this region during mining and can be pushed out from this neighborhood after mining. Moreover many other possibilities for mining exist, like moving the asteroid to the Moon's neighborhood or to Earth-Moon libration points with no further cost at all. Other libration point orbits could be considered as a final target, but the purpose of this work is quite broad in the number of asteroids analyzed. Even that some reward could be obtained looking for a specific

target libration point orbits for each case, the major numbers of this study would not change much.

Considering the time of technical development and the period of mission, the departure epoch for the asteroid has been set between March 2012 (more precisely JD 2456000.5) and February 2023 (JD 2460000.5) while the maximum transfer time considered is 1800 days.

This paper is organized as follows. Section 2 is dedicated to prune the asteroids from the Near Earth Asteroids database and to select the ones that are small and close enough to the Earth. The objective is to find a feasible continuous-thrust trajectory with a technology already validated like Variable Specific Impulse Magneto-plasma Rocket (VASIMR) [9] engines in the range of 5 N. The mass of the asteroids is a parameter which is very difficult to be well known but is essential for the trajectory computation and this section discusses different ways to estimate it. Section 3 focuses on getting a rough departure epoch and time of flight using a global optimization method based on propagating the trajectory both forward and backward in time to a middle point. Section 4 describes the methodology to further refine the initial estimated trajectories and to optimize them. Finally, the results of the trajectory optimization are summarized and discussed in section 5.

2. Asteroids Database Selection

In this research we use the JPL's Solar System Dynamics Group small-body database (SBDB) to select the asteroids and to get their orbital elements and stellar magnitude. As of 5th of September of 2012, 9049 NEAs (Near Earth Asteroids) have been identified.

First we start with an initial pruning of the asteroids selecting the smallest ones within the Earth's neighborhood [10], in order to be possible to move them with the current technology of a Solar Electric Propulsion (SEP) system. The initial constraints in the NEAs database are: a semi-major axis range between 0.85-1.15 AU and a stellar magnitude bigger than 28. The stellar magnitude represents the brightness of the object and is directly related with its size. Applying these constraints, we get a final selection of 40 asteroids whose orbital parameters and stellar magnitude are shown in Table 1.

We note that the asteroid 2004 UH1, within the above limits, has been discarded because of its high eccentricity which implies a high relative speed with respect to the Earth and big maneuvers for the capture.

Name	H	a [AU]	e	i [deg]	Ω [deg]	ω [deg]	M [deg]	n [deg/day]
1991 VG	28.39	1.03	0.0491	1.45	73.98	24.51	340.17	0.95
2000 LG6	29.02	0.92	0.1109	2.83	72.55	8.19	185.75	1.12
2003 SW130	29.12	0.88	0.3043	3.67	176.45	47.80	49.55	1.19
2003 WT153	28.05	0.89	0.1777	0.37	55.61	148.91	55.61	1.17
2006 BV39	28.98	1.15	0.2714	0.74	127.09	74.96	116.33	0.80
2006 JY26	28.35	1.01	0.0830	1.44	43.50	273.45	29.55	0.97
2006 RH120	29.53	1.03	0.0245	0.60	51.14	10.14	221.25	0.94
2007 EK	29.26	1.13	0.2724	1.21	168.58	83.26	181.71	0.82
2007 UN12	28.74	1.05	0.0605	0.24	216.11	134.34	238.24	0.91
2008 CM74	28.04	1.09	0.1469	0.86	321.58	242.73	339.86	0.87
2008 GM2	28.36	1.05	0.1572	4.10	195.11	278.25	121.93	0.91
2008 HU4	28.22	1.09	0.0733	1.26	221.34	341.50	327.11	0.86
2008 JL24	29.57	1.04	0.1066	0.55	225.82	281.97	124.19	0.93
2008 KT	28.22	1.01	0.0848	1.98	240.66	101.86	7.44	0.97
2008 LD	28.86	0.89	0.1547	6.54	250.90	201.42	202.43	1.17
2008 UA202	29.44	1.03	0.0686	0.26	21.06	300.89	330.08	0.94
2008 UC202	28.24	1.01	0.0685	7.46	37.43	91.24	230.71	0.97
2008 WO2	29.78	1.03	0.1882	2.01	238.15	85.70	331.19	0.95
2009 BD	28.24	1.06	0.0516	1.27	253.33	316.73	115.11	0.90
2009 WQ6	29.19	0.87	0.4087	5.82	55.68	227.27	288.88	1.22
2009 WW7	28.89	1.09	0.2618	2.53	57.18	273.71	241.39	0.87
2009 WR52	28.32	1.03	0.1551	4.24	61.03	269.88	329.31	0.94
2009 YR	28.00	0.94	0.1102	0.70	86.95	127.87	257.46	1.08
2010 JW34	28.15	0.98	0.0548	2.26	49.81	43.61	294.67	1.01
2010 RF12	28.37	1.06	0.1882	0.88	163.85	267.56	254.92	0.90
2010 UY7	28.53	0.90	0.1499	0.46	39.95	210.44	228.37	1.16
2010 UE51	28.31	1.06	0.0597	0.62	32.29	47.25	239.36	0.91
2010 VL65	28.42	1.07	0.1440	4.40	223.12	253.97	203.68	0.90
2010 VQ98	28.20	1.02	0.0271	1.48	46.17	341.60	316.69	0.95
2011 AM37	29.69	1.10	0.1473	2.63	291.28	129.20	213.92	0.85
2011 BQ50	28.34	0.95	0.0982	0.36	281.01	1.27	141.56	1.06
2011 CA7	30.32	1.08	0.2888	0.12	311.00	278.61	108.09	0.88
2011 CH22	28.96	0.88	0.2358	0.13	334.67	27.59	115.28	1.20
2011 JV10	29.71	1.14	0.2020	1.40	221.39	297.52	101.68	0.81
2011 MD	28.07	1.06	0.0371	2.45	271.63	5.84	56.38	0.91
2011 UD21	28.48	0.98	0.0302	1.06	22.52	208.45	144.91	1.02
2012 AQ	30.70	1.07	0.1038	2.86	97.32	316.09	280.99	0.89
2012 EP10	29.17	1.05	0.1160	1.03	348.04	105.73	249.95	0.92
2012 FS35	30.29	1.10	0.1185	2.34	186.57	42.23	126.35	0.86

Table 1: Orbital Elements and stellar magnitude of NEAs selected (5^{th} Sept 2012).

The vast majority of the selected asteroids are from the Apollo family, which have a semi-major axis greater than 1 AU and a perihelion distance $q < 1.017$ AU. In fact, 38 out of the 39 selected NEAs cross the Earth's orbit and they are either Apollo or

Aten. The other one belongs to the Amor family ($1 < q < 1.3$ AU and $a > 1$ AU). The highest inclination with respect to the ecliptic of those asteroids selected is 7.45 deg and the eccentricity range is between 0.0244 and 0.4086.

2.1. Mass Estimation

The mass of an asteroid is a difficult parameter to be determined. Only close measurements or special observed dynamics like spacecraft tracking during encounters or natural satellites of asteroids [11] could provide high accuracy. Since this is not available, in this work we estimate it by means of first estimating the diameter of the NEA using two different methods. Then, we assume an spherical shape of the asteroids and a bulk density [12] of 2.6 g/cm^3. Note that this density value is again an estimation based on a weighted mean using a population fraction and absolute magnitude and the only way to accurately know it is to send a probe to the NEA.

In the first method to determine the diameter we consider the relationship between the observed absolute magnitude and the diameter of the asteroid stated in JPL [1] which assumes an albedo ranging from 0.25 to 0.05. This method classifies the asteroids based on its absolute magnitude and, in practice, we put them in five groups: Group A: $28 < H < 28.3$; Group B: $28.3 < H < 28.7$; Group C: $28.7 < H < 29.3$; Group D: $29.3 < H < 29.7$; Group E: $29.7 < H < 30.2$. Then, for instance, asteroid 1991 VG which has a stellar magnitude of 28.39 belongs to group B, and using this method, in the lower limit we obtain a mass of 170169 kg while in the upper one we obtain 2352424 kg. The range of diameters and stellar magnitudes is directly obtained from JPL's data and summarized in Table 2.

Group	H	D [m]	Mass [Kg]
A	28	$7-15$	466945 - 4594579
B	28.5	$5-12$	170169 - 2352424
C	29	$4-9$	87126 - 992429
D	29.5	$3-7$	36756 - 466945
E	30	$3-6$	36756 - 294053

Table 2: NEAs Method 1 classification and the relationship between absolute magnitude H, diameter D and Mass.

In the second method we consider Fowler and Chillemi [13]. Following their work,

we have the relation,

$$D = \frac{1329}{\sqrt{p_v}} 10^{-0.2H}, \tag{1}$$

where H is the absolute magnitude, taken again from the SBDB database and p_v is the geometric albedo, considered in the range [0.05, 0.5] according to [14].

Table 3 summarizes the range of values derived from this second method of estimation. It is interesting to compare the values obtained with the two methods. In the lower limit the difference in diameter can be up to 37 %, while in the upper one it is only 6.5 %. If we compare masses, we notice that the lower limit is quite different since we have considered an albedo of 0.25 in Method 1 and of 0.5 in Method 2.

H	D [m]	Mass [Kg]
28	$4.72 - 14.93$	143249 - 4529934
28.5	$3.75 - 11.86$	71794 - 2270345
29	$2.98 - 9.42$	35982 - 1137868
29.5	$2.37 - 7.48$	18033 - 570284
30	$1.88 - 5.94$	9038 - 285819

Table 3: NEAs Method 2 relationship between absolute magnitude H, diameter D and Mass considering an albedo range of [0.05, 0.5].

At the end, we have two absolute limits for diameter and mass reflecting someway the uncertainty of their determination, but also the range that the mission could find. In this work, we have performed the computations for the four limiting cases, two for each mass determination method. For the first one we consider the limiting masses of Table 2 and for the second one the limiting masses obtained using Eq. 1 and albedos of 0.05 and 0.5.

In the following sections we describe the procedure we implement to compute the capture trajectories. Since efficiency in convergence is required due to the number of asteroids and cases explored, it goes through a number of steps to find out optimal trajectories in a systematic way.

3. Global Search Step

In order to find the potential mining targets, a large number of fuel optimal continuous-thrust trajectories have to be computed. Hence, a fast algorithm to generate good first

estimations for these trajectories is of major interest to assure systematic convergence in further refinements. Our initial estimate generation algorithm is based on the impulses approximation model introduced by Sims and Flanagan [15]. In this model, continuous-thrust trajectories are approximated by means of Kepler trajectory arcs series connected by small impulses (see Fig. 1). This model considers the two-body gravitational field and trajectories are generated using forward and backward propagations. Assuming a departure epoch, t_L, a time of flight, TOF, and a set of 60 impulses ($j+k=30+30$), $\Delta V_i,\ i=1,2,\ldots,j+k$. The trajectory is generated using the following procedure:

(1) Compute the initial state of the NEA using the departure epoch, t_L, and its orbital elements.

(2) Use this initial state for the NEA and the series of impulses, $\Delta V_i,\ i=1,2,\ldots,j$, to perform a Keplerian forward propagation.

(3) Compute the state of the Sun-Earth L_2 libration point at time t_L+TOF using the JPL ephemeris. Essentially L_2 is identified along the Sun-Earth line keeping the same proportions of distances as in the RTBP (see the change of coordinates $\vec{e}=kC\vec{a}+\vec{b}$ between RTBP coordinates and JPL ones in [16] pag 138).

(4) Use the state of the Sun-Earth L_2 libration point and the series of impulses, $\Delta V_i,\ i=j+1,j+2,\ldots,j+k$, to perform a Keplerian backward propagation.

We remark that the impulsive maneuvers $\Delta V_i,\ i=1,2,\ldots,j+k$ are determined by parameters α_i, β_i and k_i, which represent the direction and the magnitude of the thrust:

$$\Delta V_i=\Delta V_{\max}k_i[\cos\beta_i\cos\alpha_i,\cos\beta_i\sin\alpha_i,\sin\beta_i]^T$$

where $\alpha_i\in[0,2\pi)$, $\beta_i\in[-\frac{\pi}{2},\frac{\pi}{2}]$, $k_i\in[0,1]$. The ΔV_i should not exceed the maximum magnitude $\Delta V_{\max}=at_{step}$, where a is the acceleration offered by the continuous-thrust engine when operated at full thrust and t_{step} is the time span between the two nodes. In our computations, the maximum magnitude of the acceleration has been set to 10^{-4} m/s^2. We also note that the forward segment and the backward segment may not connect with each other. The position error and the velocity error are denoted by $\mathbf{R}_{conn}$ and $\mathbf{V}_{conn}$, respectively. The fuel optimal trajectory in this impulsive

approximation model is then determined solving an unconstrained parameter optimization problem with a set of parameters $\mathbf{z} = [t_L, TOF, k_i, \alpha_i, \beta_i],\ i = 1, 2, \ldots, j+k$, and the objective to minimize,

$$J(\mathbf{z}) = \sum_{i=1}^{j+k} k_i + \lambda_r ||\mathbf{R}_{conn}||_2 + \lambda_v ||\mathbf{V}_{conn}||_2 \tag{2}$$

where λ_r and λ_v are weight factors. $\mathbf{R}_{conn}$ and $\mathbf{V}_{conn}$ is conveniently expressed in canonical units, where the unit of distance is measured in AU and the velocity in VU. The weight factors affect the feasibility and optimality of the trajectory we find. For high weight parameters the optimizer focuses more on the constraints rather than in the maneuvers. In our computations, both λ_r and λ_v are set to 10^5.

To obtain this first global optimal solution estimate, we address the problem by means of a differential evolution (DE) algorithm, which is a kind of meta-heuristics procedure first introduced by Storn and Price [17] and detailed in Table 4 (see also [18, 19] for some implementations). DE makes no assumptions about the problem being optimized and it can search inside very large spaces of candidate solutions. In our computations we take the weight factor $F = 0.8$ and a crossover constant $CR = 0.8$. For each run, the number of maximum iterations has been set to 20000 and the population size to 50. In DE, all the optimization parameters have to be considered inside $[0, 1]$; hence, we cast $\mathbf{z}$ into $[\widehat{t}_L, \widehat{TOF}, k_i, \xi_i, \rho_i]^T$, where

$$\widehat{t}_L = \frac{t_L - t_L^-}{t_L^+ - t_L^-}, \quad t_L \in [t_L^-, t_L^+]$$

$$\widehat{TOF} = \frac{TOF - TOF^-}{TOF^+ - TOF^-}, \quad TOF \in [TOF^-, TOF^+]$$

$$\xi_i = \frac{\alpha_i}{2\pi}, \ \ \rho_i = \frac{\beta_i + \pi/2}{\pi}$$

The departure epoch in our problem has been set between JD 2456000.5 and 2460000.5 and the time of flight between 200 and 1800 days. Then $t_L^- = 2456000.5$, $t_L^+ = 2460000.5$, $TOF^- = 200$ and $TOF^+ = 1800$.

In most cases DE obtains a solution in less than 4 minutes working on a GNU-Linux box dual core Intel Xeon 3.2 GHz processor. But sometimes the position and velocity mismatches at the connection point are rather big. In fact, the velocity mismatch can be bigger than $\Delta V_{\max}$, meaning that this initial trajectory of the impulses

Require:

Input parameters of the basic DE algorithm are $\mathbf{X}^L$, $\mathbf{X}^U$, NP, F, CR, $\text{Iter}_{\max}$ where $\mathbf{X}^L$ and $\mathbf{X}^U$ are the lower and upper bounds of the optimization parameters. NP is the population number. F is called differential weight, and CR is called crossover probability, $\text{Iter}_{\max}$ is the maximum number of iteration. $\text{Iter} = 0$

Initialize all agents $\mathbf{X}_k,\ k = 1, \ldots, NP$ with random positions in the search-space.

Ensure:

while $\text{Iter} \leq \text{Iter}_{\max}$ **do**
  $\text{Iter} = \text{Iter} + 1$
  for $(k = 1, i \leq NP, i++)$ **do**
    Pick three agents $\mathbf{a}$, $\mathbf{b}$ and $\mathbf{c}$ from the population at random. They must be distinct from each other as well as from agent $\mathbf{X}_k$.
    Pick random index $R \in \{1, \ldots, n\}$, where n is the dimension of the optimization problem.
    Compute the agent's potentially new position $\mathbf{Y} = [y_1, \ldots, y_n]$ as follows:
    for $(i = 1, i \leq n, i++)$ **do**
      Pick a uniformly distributed number $r_i \equiv U(0, 1)$.
      if $r_i < CR$ or $i = R$ **then**
        $y_i = a_i + F(b_i - c_i)$
      else
        $y_i = x_i$
      end if
    end for
    $\mathbf{Y} = [y_1, \ldots, y_n]$
    if $f(\mathbf{Y}) < f(\mathbf{X}_k)$ **then**
      $\mathbf{X}_k = \mathbf{Y}$
    end if
  end for
end while
Pick the agent from the population that has the highest fitness or lowest cost and return it as the best found candidate solution.

Table 4: Basic Differential Evolution algorithm

approximation model is not feasible. The connection mismatches could be further decreased by increasing the maximum iterations and the population size of DE, or using the local optimizer, but the computational effort would increase as well. Nevertheless, it is meaningless to have a high accurate trajectory in this approximate model and further optimizations have been discarded. We only use the t_L and TOF output of this step as a direct initial guess for the following one.

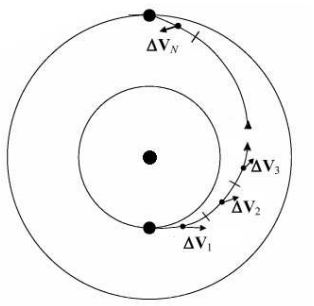

Figure 1: Impulses approximation model [18].

4. Optimal Trajectory Generation

The method described in the previous section provides us with estimates of departure epoch, t_L, and time of flight, TOF. Now, using the orbital elements of the selected NEAs and the JPL ephemeris, the initial and final states of the continuous-thrust transfer trajectory can be obtained and, so far, a continuous-thrust Lambert problem is defined. The continuous-thrust Lambert problem has been investigated by many researchers, and two types of algorithms (direct and indirect methods) are available. Anyway, the main difficulty of this problem is the strong sensitivity of the dynamics. A tiny deviation of the initial guess can lead to the divergence of the algorithm. Long times of flight and small thrust accelerations increase the sensitivity of the system, and unfortunately, in our application of asteroid mining, the SEP system will be used to change the orbit of NEA, whose mass is far much bigger than the one of a standard spacecraft. Due to this tiny acceleration generated by the SEP system, to solve the continuous-thrust Lambert problem is not an easy task. The procedure in this section is divided in two steps: an accurate initial guess detection and a final local optimization phase. In the first step we generate a series of control histories using a random multi-point start technique for the conjugated equations. The second part uses a 4^{th} order Runge-Kutta shooting method to refine and locally optimize the control sequences. The result which achieves the best performance is chosen as a final output.

4.1. Accurate initial guess detection

Here we introduce the usual dynamical equations expressed in cartesian coordinates, the conjugated equations and the optimal control conditions to obtain the initial seed of the final optimization problem. We remark that in this new step the mass equation is also propagated along the trajectory, while in the previous global search step it was assumed constant along the trajectory. Then, the vector-field is given by,

$$\begin{aligned}
\dot{\mathbf{r}} &= \mathbf{v} \\
\dot{\mathbf{v}} &= -\frac{\mu}{r^3}\mathbf{r} + \frac{T}{m}\boldsymbol{\gamma} \\
\dot{m} &= -\frac{T}{g_0 I_{sp}} \\
\dot{\boldsymbol{\lambda}}_r &= \boldsymbol{\lambda}_v \frac{\mu}{r^3} - \frac{3\boldsymbol{\lambda}_v^T \mathbf{r}}{r^5}\mathbf{r} \\
\dot{\boldsymbol{\lambda}}_v &= -\boldsymbol{\lambda} \\
\dot{\lambda}_m &= -||\boldsymbol{\lambda}_v|| \frac{T}{m^2}
\end{aligned} \tag{3}$$

where the Thrust T and the variable $\boldsymbol{\gamma}$ are the control parameters. In this case our performance index is defined as

$$J = \frac{m_f}{m_0} \longrightarrow \max \tag{4}$$

where, m_0 and m_f are respectively the initial and final masses of the spacecraft-asteroid assembly. Applying Pontryagin's maximum principle, the optimal control is given by,

$$\boldsymbol{\gamma} = -\frac{\boldsymbol{\lambda}_v}{||\boldsymbol{\lambda}_v||}$$

and T is determined by the switch function,

$$H_T = -\frac{||\boldsymbol{\lambda}_v||}{m} - \frac{\lambda_m}{g I_{sp}} \tag{5}$$

$$\begin{aligned}
T &= 0 && \text{if} \quad H_T > 0 \\
T &= T_{\max} && \text{if} \quad H_T < 0 \\
0 &< T < T_{\max} && \text{if} \quad H_T = 0
\end{aligned}$$

where $g = 9.81$ m/s^2 and $I_{sp} = 3000$ s. T_{max} is the value when the engine operates at full thrust and it depends on the particular case computed.

A direct method would have not needed the conjugated equations (Eq. 3), but in our research we consider more convenient to work with conjugated equations in order to generate initial guesses for the piecewise continuous time history of control. The procedure we implement is as follows:

(1) We randomly generate initial values of the conjugated states $[\boldsymbol{\lambda}_r^T, \boldsymbol{\lambda}_v^T, \lambda_m]$, setting the limits of them between -100 and 100 to have the same order of magnitude.

(2) We use these initial values, the departure epoch and the time of flight obtained from the global search step of section 3, to propagate the initial states in the vector-field (Eq. 3).

(3) If the error of the final states is smaller than a given tolerance (position error less than 0.5 AU and velocity error less than 0.2 VU), the set of initial conjugated states $[\boldsymbol{\lambda}_r^T, \boldsymbol{\lambda}_v^T, \lambda_m]$ is accepted, otherwise it is rejected and steps 1-3 are repeated until a set of accepted conjugated states is obtained.

(4) Finally, we generate the discrete time history of control using the control equation and switch function (Eq. 5). In all computations the number of nodes used is 101 (corresponding to 50 stages).

Using this procedure we obtain a series of trajectories whose final states are not very far from the target state. Also the time history of control is also obtained. In our research we compute 50 sets of control histories for each transfer orbit. We denote each set of discretized control history in the form $[\mathbf{u}_0, \mathbf{u}_1, \ldots, \mathbf{u}_p],\ p \in \mathbb{Z}$, where $\mathbf{u}_i = [\alpha_i, \beta_i, T_i]$.

We note that we do not include the Earth's gravitational field in our vector-field equations. Even that for more realistic computations, and for selected particular cases, this and other perturbations had to be taken into account, the Earth's influence should not play a significative role with regard to our final estimations of ΔV needed for the transfer. Different from other specific libration point missions, or for the station keeping about a libration point orbit, where the ΔV expenditure is at least one or two orders of magnitude less, moreover the spacecraft remains most of the time in the libration point region, in our case the impact on the final result is proportionally much lower. This is because most of the time the satellite is very far from the Earth, and

even near the libration region is outside of the Earth's sphere of influence. Since our target is to obtain major numbers to evaluate the cost for a large number of NEAs and quite open range of mass estimations, it is not relevant to get very accurate orbits that would include other minor perturbations. Moreover the computational effort for our exploration would increase noticeably.

4.2. Final local optimization phase

In order to obtain the final transfer trajectories, we use a local optimizer to deal with the discretized control sequences of the previous accurate initial guess detection. The problem is formulated in terms of a parameter optimization problem defined by,

$$\max_{[\alpha_i,\beta_i,T_i]^T} m(t_f), \quad i = 0, 1, \cdots, p, \tag{6}$$

and restricted to the conditions,

$$[\mathbf{r}(t_f) - \mathbf{r}_f, \mathbf{v}(t_f) - \mathbf{v}_f]^T = \mathbf{0}, \tag{7}$$

$$\alpha_i \in [0, 2\pi], \quad \beta_i \in [-\frac{\pi}{2}, \frac{\pi}{2}], \quad T_i \in [0, T_{\max}]. \tag{8}$$

In Eq. 6, $m(t_f)$ is the final mass of the NEA with the spacecraft. In Eq. 7, $\mathbf{r}(t_f)$ and $\mathbf{v}(t_f)$ denote the final states obtained by numerical integration, while $\mathbf{r}_f$ and $\mathbf{v}_f$ are the terminal constraints computed using JPL ephemeris (the state of the L_2 libration point). The Jacobian matrix of the terminal constraints (see Eq. 7) with respect to the optimization parameters is,

$$\left[\begin{array}{ccc|c|ccc} \frac{\partial \mathbf{r}(t_f)}{\partial \alpha_0} & \frac{\partial \mathbf{r}(t_f)}{\partial \beta_0} & \frac{\partial \mathbf{r}(t_f)}{\partial T_0} & \cdots & \frac{\partial \mathbf{r}(t_f)}{\partial \alpha_p} & \frac{\partial \mathbf{r}(t_f)}{\partial \beta_p} & \frac{\partial \mathbf{r}(t_f)}{\partial T_p} \\ \hline \frac{\partial \mathbf{v}(t_f)}{\partial \alpha_0} & \frac{\partial \mathbf{v}(t_f)}{\partial \beta_0} & \frac{\partial \mathbf{v}(t_f)}{\partial T_0} & \cdots & \frac{\partial \mathbf{v}(t_f)}{\partial \alpha_p} & \frac{\partial \mathbf{v}(t_f)}{\partial \beta_p} & \frac{\partial \mathbf{v}(t_f)}{\partial T_p} \end{array}\right]_{6\times 3(p+1)} \tag{9}$$

while the Jacobian matrix of the performance index with respect to the optimization parameters is,

$$\left[\begin{array}{ccc|c|ccc} \frac{\partial m(t_f)}{\partial \alpha_0} & \frac{\partial m(t_f)}{\partial \beta_0} & \frac{\partial m(t_f)}{\partial T_0} & \cdots & \frac{\partial m(t_f)}{\partial \alpha_p} & \frac{\partial m(t_f)}{\partial \beta_p} & \frac{\partial m(t_f)}{\partial T_p} \end{array}\right]_{1\times 3(p+1)} \tag{10}$$

We note that the elements in this Jacobian matrix are also computed analytically.

In this final optimization we integrate the trajectory using a 4$^{\text{th}}$ order Runge-Kutta method with a fixed step-size. A high enough accuracy can be achieved using a small

step-size. However, the main task of our computations is to search inside large spaces of candidate solutions in a short period of time, hence, the value of $p = 100$ has been taken. This means that the step-size varies between 2.5 and 22.5 days, depending on the case. Moreover, using the 4^{th} order Runge-Kutta integral formula, the analytical expressions of the derivatives Eq. 9 and Eq. 10 can be implemented and this accelerates the optimization procedure in a remarkable way [20]. In our research, the optimal parameters of the problems are obtained using the sequential quadratic programming (SQP) implemented in SNOPT [21]. We note that all the 50 sets of control history of each case are refined using this SQP algorithm. The one that achieves the best performance is the one selected as optimal solution. This way to proceed is called multi-point start technique. This technique increases the probability of convergence, and it also imports a global search behavior into the algorithm.

5. Results

In the previous sections the methodology we implement to capture NEAs has been described. In this section we present the details of the computations and we discuss the results with several graphics as well as the presentation of an specific example.

The transfer opportunity search has been done one time for each asteroid, needing about 4 minutes each. Concerning the computations of section 4, a total of 156 trajectories have been computed. They account for 39 selected asteroids with two mass estimation methods and two mass range boundaries for each one. The computational time of the trajectory generation strongly depends on the time of flight. For instance, for the 2010 UY7 asteroid with Method 2 upper limit mass estimation case (TOF = 1110 days), the time needed when executed in a dual core Intel Xeon 3.2 GHz CPU is 13 minutes. However, the case of 2012 FS35 Method 2 lower mass limit (TOF = 255 days) only needed one minute and a half.

The outputs from the global search step method (listed in Table 5 of the Appendix) are considered rough estimates for two reasons. First, in some cases the method described in Section 4 did not converge using directly the outputs (t_L and TOF). Therefore, we decided to change the time of flight estimation input from 6 to 33 Time Units

(TU) ($348.79 - 1918.37$ days) with a time step of 3 TU, which is approximate one orbit. The result of convergence with the lowest time of flight is the one shown in Tables from 6 to 9 in the Appendix. Second, these final output parameters also differ from the global search step initial ones because the transfer of the asteroid is considered from the first time that the engine starts until it stops for the last time. Therefore, since the control profile we have obtained is different for each method, the time of flight and departure epoch seems to vary. Anyway, we remember that the objective function in this research is the maximization of the final mass.

In the optimal trajectory optimization problem, the thrust value $T_{\max}$ of the engine is another input parameter. The criteria that we have applied is to start with the lowest one (5 N) and to search if changing the time of flight as we discussed before, the problem converges to a solution. Otherwise, we increased the thrust with a 5 N step.

In Figures 2, 3 and 4 we present a summary of the main output results of the research. The dependence of the total $\triangle V$ of the transfer with respect to the NEAs mass is shown in Fig. 2 and the relationship of the $\triangle V$ with respect to the thrust needed is in Fig. 3. As a figure of merit, it can be seen that 70% of the NEAs selected have a transfer cost below 4 km/s to be captured at L_2.

As we can see in Fig. 3, the thrust needed in the lowest mass estimation limit is between the range $5 - 25$ N. However, in the upper limit mass cases the thrust could be much bigger, in the range between $15 - 200$ N. This one order of magnitude difference is obviously due to the mass estimated increment. Therefore, if the asteroids would be near the lower limit of the mass estimation in Method 2, using only one VASIMR engine would be enough to capture them. Otherwise, more than one engine can be required.

In Fig. 4, we show the time of flight related with the time the thruster is on. In the lower limit mass case the thruster is more than 60% on in 21% and 23% of the time for Method 1 and 2 respectively of the asteroids analyzed, while in the upper limit case, the asteroids which need the time on increase to 67% and 54%. Of course, this is an interesting output because it gives us an idea of the real cost of the transfer. In 6 out of 156 computed cases the thruster is on maximum 15% of the time of flight. Two of these computed results correspond to the asteroid 2006 RH120: one case in lower limit

mass estimation Method 1 and the other case in Method 2 upper limit. The other four are 2007 UN12, 2008 JL24, 2008 UA202 and 2012 EP10; all of them with Method 1 lower mass estimation limit. The mass estimated of those asteroids is below 2000 kg.

Looking at the cost, the asteroids which would be suitable to capture considering any of the estimated mass method are 1991 VG, 2007 UN12, 2010 VQ98, 2011 UD21 because they would only need about 1.5 km/s of $\triangle V$.

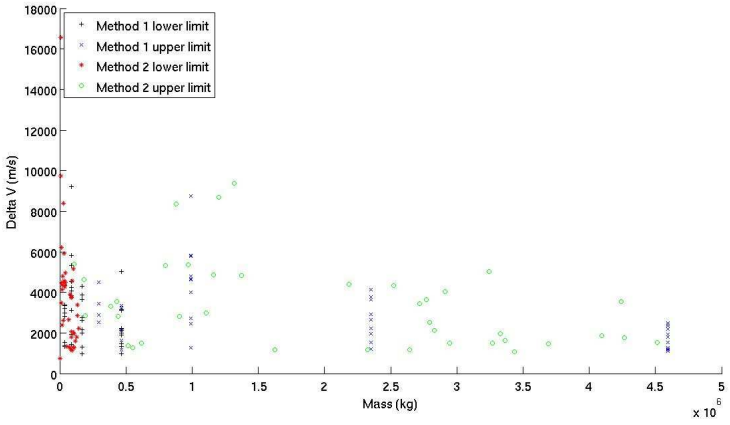

Figure 2: Estimation of $\triangle V$ needed to capture one asteroid of a certain mass. The figure contains the results for all the cases studied (see Tables 6, 7, 8 and 9 in the Appendix).

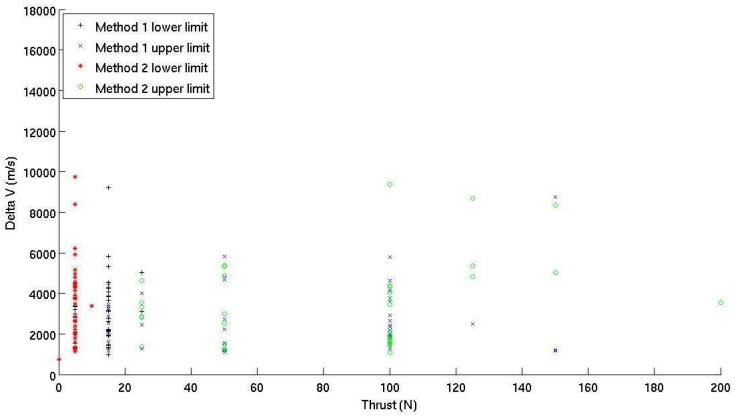

Figure 3: Relationship between the Thrust needed versus the $\triangle V$ for all the cases studied in this research (see Tables 6, 7, 8 and 9 in the Appendix).

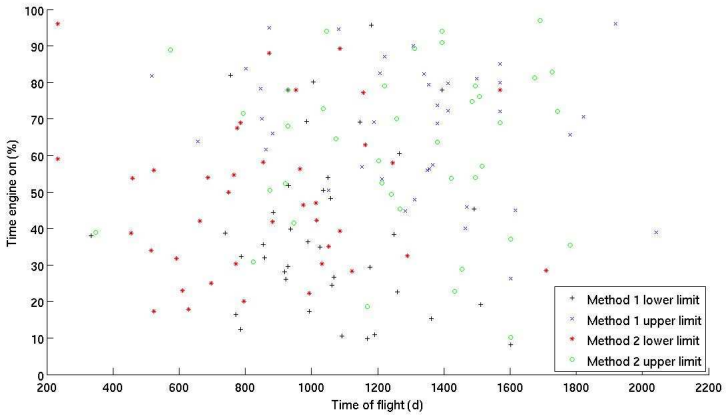

Figure 4: Relationship between the time of flight and the duration where the thruster is on for all the cases studied in this research (see Tables 6, 7, 8 and 9 in the Appendix).

5.1. Asteroid 2011 MD

To further illustrate the results, in this subsection we show the output corresponding to the particular transfer of asteroid 2011 MD that is quite representative of many transfers computed. In Fig. 5 the trajectory is plotted, while in Fig. 6 there is the thrust profile. As we discussed before, the thruster follows an on-off profile. The figures pre-

sented correspond to the application of JPL mass estimation method (Method 1) in the lower limit. In order to capture the asteroid assuming a thrust equal to 15 N, it would take about 985 days with the thruster on during almost 70% of the mission length. The accumulated $\triangle V$ for this case would be about 1900 m/s.

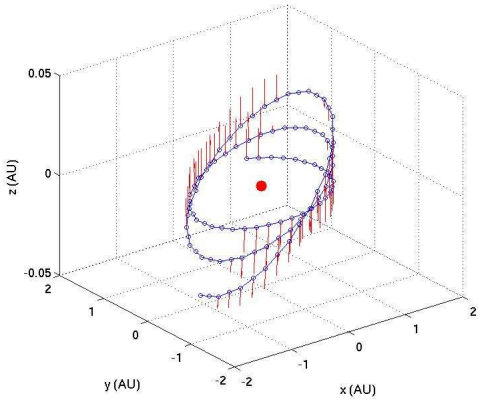

Figure 5: Capture trajectory for asteroid 2011 MD (Method 1, lower mass limit).

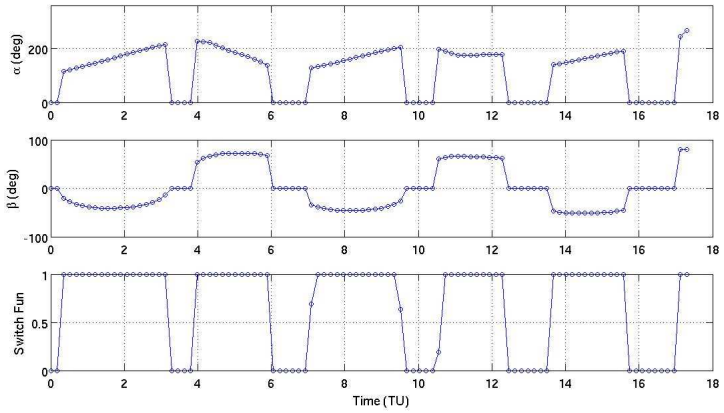

Figure 6: Thrust profile for asteroid 2011 MD maneuvering phase (Method 1, lower mass limit).

6. Conclusions

In this research we have addressed a procedure to capture asteroids into the Sun-Earth L_2 libration point. The method follows several steps, starting from a global search step, followed by a random initial guess trajectory and ending with an optimal refined on-off continuous-thrust control. A list of candidates and opportunities has been identified and the main parameters describing their trajectories are shown. The method is very robust and convergent solutions have been found for all asteroids including the two mass estimation methods with the two mass limiting boundaries.

Acknowledgements

This work has been supported by the MICINN/FEDER grants MTM2009-06973, MTM2010-16425 and MTM2012-31714. The Catalan grant 2009SGR859 and the FP7 European Marie Curie PITN-GA-2011-289240. We acknowledge the comments of three anonymous referees that helped to improve this manuscript. We also acknowledge the use of the UPC Applied Math cluster system for research computing

(see http://www.ma1.upc.edu/eixam/index.html).

Appendix

In Tables 5, 6, 7, 8 and 9 of this appendix we list the results presented in section 5 for all the NEAs selected and studied in this work.

Global Search Step					
Name	DT_{GO} [JD]	TOF_{GO} [d]	Name	DT_{GO} [JD]	TOF_{GO} [d]
1991 VG	2457589.62	977	2009 WW7	2457444.51	1193
2000 LG6	2458636.74	1498	2009 WR52	2456024.82	1154
2003 SW130	2456128.74	912	2009 YR	2458046.12	1221
2003 WT153	2456220.47	1570	2010 JW34	2456006.76	929
2006 BV39	2457303.08	1192	2010 RF12	2459962.67	1499
2006 JY26	2456976.17	1500	2010 UY7	2456970.35	1279
2006 RH120	2460000.50	1619	2010 UE51	2459989.98	574
2007 EK	2458014.42	1221	2010 VL65	2458982.79	1245
2007 UN12	2458639.10	883	2010 VQ98	2456000.50	1046
2008 CM74	2457264.83	1257	2011 AM37	2457412.01	1307
2008 GM2	2458974.37	1453	2011 BQ50	2459410.93	1084
2008 HU4	2457224.88	1279	2011 CA7	2458886.04	1064
2008 JL24	2459947.31	1629	2011 CH22	2456895.09	1119
2008 KT	2456408.20	1046	2011 JV10	2458967.43	1351
2008 LD	2459989.80	986	2011 MD	2460000.50	1006
2008 UA202	2459999.64	1444	2011 UD21	2456000.50	1226
2008 UC202	2460000.50	1395	2012 AQ	2458872.57	1337
2008 WO2	2456000.50	1800	2012 EP10	2456000.75	1453
2009 BD	2459425.83	1046	2012 FS35	2458396.83	1213
2009 WQ6	2457438.15	1570			

Table 5: Results of the global search step (departure epoch (DT_{GO}) and time of flight (TOF_{GO})) for the 39 pruned asteroids ($H > 28$ and $0.85 <$semi-major axis< 1.15).

Method 1:	Lower Limit Results					
Name	T [N]	a $[m/s^2]$	DT [JD]	TOF [d]	T_{ON} [d]	$\triangle V$ [m/s]
1991 VG	15	8.81E-005	2457591.64	771.70	126.99	967
2000 LG6	15	1.72E-004	2458638.80	1363.25	209.73	3117
2003 SW130	15	1.72E-004	2456128.90	884.98	392.31	5830
2003 WT153	25	5.35E-005	2456220.47	1491.10	674.92	3120
2006 BV39	15	1.72E-004	2457304.51	858.40	274.21	4075
2006 JY26	15	8.81E-005	2456980.30	1260.00	285.00	2169
2006 RH120	5	1.36E-004	2460000.50	1602.35	129.48	1521
2007 EK	15	1.72E-004	2458016.94	854.55	305.20	4536
2007 UN12	15	1.72E-004	2458639.71	786.15	97.16	1444
2008 CM74	15	3.21E-005	2457266.12	1181.23	1130.97	3137
2008 GM2	15	8.81E-005	2458977.62	1249.85	479.59	3651
2008 HU4	15	3.21E-005	2457224.88	1266.12	767.35	2128
2008 JL24	5	1.36E-004	2459955.43	1091.26	114.01	1340
2008 KT	15	3.21E-005	2456408.92	1004.53	805.72	2235
2008 LD	15	1.72E-004	2459992.17	739.34	285.88	4248
2008 UA202	5	1.36E-004	2460002.13	1169.51	115.51	1357
2008 UC202	25	5.35E-005	2460000.50	1395.18	1088.24	5030
2008 WO2	5	1.36E-004	2456005.45	1511.64	287.93	3383
2009 BD	15	3.21E-005	2459427.81	931.28	481.34	1335
2009 WQ6	15	1.72E-004	2457438.15	755.72	619.69	9209
2009 WW7	15	1.72E-004	2457446.36	1025.97	357.90	5319
2009 WR52	15	8.81E-005	2456026.61	1050.57	565.69	4306
2009 YR	15	3.21E-005	2458047.17	1147.53	793.51	2201
2010 JW34	15	3.21E-005	2456006.76	929.11	724.71	2010
2010 RF12	15	8.81E-005	2459967.57	989.44	359.80	2739
2010 UY7	15	8.81E-005	2456971.89	1176.60	345.31	2628
2010 UE51	15	8.81E-005	2459989.98	333.07	126.34	962
2010 VL65	15	8.81E-005	2458983.86	1058.37	510.51	3886
2010 VQ98	15	3.21E-005	2456000.68	1035.92	523.19	1451
2011 AM37	5	1.36E-004	2457413.81	928.08	274.50	3225
2011 BQ50	15	8.81E-005	2459411.30	1062.75	260.26	1981
2011 CA7	5	1.36E-004	2458887.32	936.52	372.48	4377
2011 CH22	15	1.72E-004	2456898.36	917.83	257.44	3826
2011 JV10	5	1.36E-004	2458967.43	1067.36	283.73	3334
2011 MD	15	3.21E-005	2460000.85	985.58	683.87	1897
2011 UD21	15	8.81E-005	2456003.88	993.29	171.68	1307
2012 AQ	5	1.36E-004	2458874.87	922.72	240.71	2828
2012 EP10	15	1.72E-004	2456005.25	1191.72	130.80	1944
2012 FS35	5	1.36E-004	2458399.55	788.56	254.76	2994

Table 6: Final results of the trajectory optimization considering the mass estimated using the lower limit of Method 1. For the 39 pruned asteroids ($H > 28$ and $0.85 <$semi-major axis< 1.15), we specify the Thrust (T), acceleration (a), departure epoch (DT), time of flight (TOF), the time where the thruster is on (T_{ON}) and the accumulated $\triangle V$ to perform the capture.

Method 1:	Upper Limit Results					
Name	T [N]	a $[m/s^2]$	DT [JD]	TOF [d]	T_{ON} [d]	$\triangle V$ [m/s]
1991 VG	50	2.13E-005	2457590.97	849.85	595.87	1097
2000 LG6	50	5.04E-005	2458638.18	1311.47	627.83	2734
2003 SW130	100	1.01E-004	2456129.19	845.83	662.71	5783
2003 WT153	150	3.26E-005	2456220.56	517.96	423.79	1194
2006 BV39	50	5.04E-005	2457303.08	1353.32	1074.29	4678
2006 JY26	50	2.13E-005	2456976.17	1500.00	1215.00	2236
2006 RH120	15	3.21E-005	2460000.50	1602.35	420.82	1167
2007 EK	25	2.52E-005	2458014.42	1918.37	1841.64	4010
2007 UN12	25	2.52E-005	2458639.10	883.32	582.99	1269
2008 CM74	100	2.18E-005	2457266.48	1822.45	1285.31	2421
2008 GM2	100	4.25E-005	2458975.77	1082.90	1024.68	3763
2008 HU4	100	2.18E-005	2457224.88	1569.58	1255.66	2365
2008 JL24	15	3.21E-005	2459949.55	1465.88	586.35	1626
2008 KT	100	2.18E-005	2456408.51	1782.00	1170.00	2204
2008 LD	50	5.04E-005	2459989.80	1569.58	1334.14	5810
2008 UA202	15	3.21E-005	2459999.89	1357.21	765.24	2122
2008 UC202	150	3.26E-005	2460000.50	655.73	418.55	1179
2008 WO2	15	5.10E-005	2456003.20	1365.53	784.79	3458
2009 BD	100	2.18E-005	2459426.96	1188.24	822.63	1549
2009 WQ6	150	1.51E-004	2457438.15	802.23	671.43	8760
2009 WW7	50	5.04E-005	2457445.47	1339.37	1102.19	4800
2009 WR52	100	4.25E-005	2456026.37	1413.07	1127.45	4140
2009 YR	125	2.72E-005	2458046.12	1220.78	1062.08	2496
2010 JW34	100	2.18E-005	2456006.76	1381.23	948.72	1787
2010 RF12	100	4.25E-005	2459962.67	1615.42	726.94	2669
2010 UY7	100	4.25E-005	2456970.80	2042.30	793.50	2914
2010 UE51	50	2.13E-005	2459989.98	871.99	828.39	1525
2010 VL65	100	4.25E-005	2458983.43	1207.79	996.11	3658
2010 VQ98	100	2.18E-005	2456001.02	1469.87	674.94	1271
2011 AM37	15	3.21E-005	2457412.01	1307.15	1176.43	3263
2011 BQ50	100	4.25E-005	2459411.49	1051.90	531.37	1951
2011 CA7	15	5.10E-005	2458886.31	1412.62	1020.22	4495
2011 CH22	100	1.01E-004	2456895.24	863.27	531.91	4642
2011 JV10	15	5.10E-005	2458967.43	1351.09	756.61	3334
2011 MD	100	2.18E-005	2460000.74	1381.23	1018.48	1918
2011 UD21	50	2.13E-005	2456000.50	1214.02	649.93	1196
2012 AQ	15	5.10E-005	2458873.49	1283.79	575.03	2534
2012 EP10	25	2.52E-005	2456000.75	1569.58	1130.09	2461
2012 FS35	15	5.10E-005	2458396.83	1152.51	655.11	2887

Table 7: Final results of the trajectory optimization considering the mass estimated using the upper limit of Method 1. For the 39 pruned asteroids ($H > 28$ and $0.85 <$semi-major axis< 1.15), we specify the Thrust (T), acceleration (a), departure epoch (DT), time of flight (TOF), the time where the thruster is on (T_{ON}) and the accumulated $\triangle V$ to perform the capture.

Method 2:	Lower Limit Results						
Name	T [N]	a $[m/s^2]$	Mass [kg]	DT [JD]	TOF [d]	T_{ON} [d]	$\triangle V$ [m/s]
1991 VG	5	5.98E-005	83578	2457591.64	771.70	234.44	1212
2000 LG6	5	1.43E-004	35050	2458636.74	685.96	370.42	4565
2003 SW130	5	1.63E-004	30612	2456130.63	766.37	419.68	5923
2003 WT153	10	7.46E-005	134058	2456221.22	776.07	523.19	3372
2006 BV39	5	1.36E-004	36787	2457304.31	882.24	369.59	4340
2006 JY26	5	5.65E-005	88449	2456979.79	1290.00	420.00	2051
2006 RH120	5	2.88E-004	17374	2460000.50	515.93	175.41	4362
2007 EK	5	1.98E-004	25194	2458015.02	662.71	279.04	4785
2007 UN12	5	9.72E-005	51463	2458639.71	794.98	159.00	1335
2008 CM74	5	3.70E-005	134987	2457266.56	1156.10	892.21	2855
2008 GM2	5	5.71E-005	87598	2458974.37	871.99	767.35	3784
2008 HU4	5	4.75E-005	105267	2457225.03	854.55	497.03	2040
2008 JL24	5	3.06E-004	16326	2459950.31	523.19	90.69	2400
2008 KT	5	4.70E-005	106437	2456408.82	1710.00	486.00	1973
2008 LD	5	1.15E-004	43420	2459989.97	975.93	453.46	4512
2008 UA202	5	2.55E-004	19593	2459999.64	592.95	188.35	4153
2008 UC202	5	4.88E-005	102540	2460000.50	1569.58	1224.27	5158
2008 WO2	5	4.08E-004	12266	2456000.50	455.76	176.72	6224
2009 BD	5	4.84E-005	103393	2459429.43	1031.55	313.38	1309
2009 WQ6	5	1.80E-004	27829	2457438.15	784.79	540.63	8393
2009 WW7	5	1.20E-004	41657	2457446.15	1014.04	477.19	4949
2009 WR52	5	5.43E-005	92064	2456026.01	1085.21	969.76	4550
2009 YR	5	3.50E-005	142657	2458046.12	1162.65	732.47	2218
2010 JW34	5	4.28E-005	116759	2456006.76	1014.99	429.02	1587
2010 RF12	5	5.81E-005	86038	2459962.67	952.21	742.93	3730
2010 UY7	5	7.23E-005	69166	2456971.82	1086.50	427.27	2669
2010 UE51	5	5.36E-005	93216	2459989.98	459.41	246.93	1144
2010 VL65	5	6.26E-005	79853	2458982.79	1245.14	722.18	3907
2010 VQ98	5	4.60E-005	108666	2456001.55	1123.12	317.40	1262
2011 AM37	5	3.60E-004	13870	2457413.09	627.83	111.61	3476
2011 BQ50	5	5.59E-005	89432	2459411.49	1051.90	368.71	1781
2011 CA7	5	8.60E-004	5817	2458886.04	232.53	223.23	16578
2011 CH22	5	1.32E-004	37974	2456897.04	749.91	374.95	4266
2011 JV10	5	3.69E-004	13567	2458967.43	610.39	140.39	4470
2011 MD	5	3.86E-005	129507	2460001.19	965.46	543.07	1812
2011 UD21	5	6.80E-005	73501	2456003.88	993.29	220.73	1297
2012 AQ	0.1	2.90E-005	3446	2458872.57	523.19	292.99	735
2012 EP10	5	1.75E-004	28648	2456000.75	697.59	174.40	2630
2012 FS35	5	8.21E-004	6088	2458396.83	232.53	137.19	9735

Table 8: Final results of the trajectory optimization considering the mass estimated using the lower limit of Method 2. For the 39 pruned asteroids ($H > 28$ and $0.85 <$semi-major axis< 1.15), we specify the Thrust (T), acceleration (a), departure epoch (DT), time of flight (TOF), the time where the thruster is on (T_{ON}) and the accumulated $\triangle V$ to perform the capture.

Method 2:	Upper Limit Results						
Name	T [N]	a $[m/s^2]$	Mass [kg]	DT [JD]	TOF [d]	T_{ON} [d]	$\triangle V$ [m/s]
1991 VG	50	1.89E-005	2642968	2457589.62	928.00	722.86	1182
2000 LG6	50	4.51E-005	1108388	2458638.03	1423.17	764.02	2978
2003 SW130	125	1.29E-004	968037	2456130.72	920.82	481.34	5370
2003 WT153	200	4.72E-005	4239278	2456221.22	1515.84	866.20	3531
2006 BV39	50	4.30E-005	1163300	2457303.08	1395.18	1311.47	4870
2006 JY26	50	1.79E-005	2796996	2456976.17	1691.65	1639.33	2532
2006 RH120	50	9.10E-005	549404	2460000.78	1602.35	161.85	1273
2007 EK	50	6.28E-005	796695	2458014.42	1046.38	983.60	5333
2007 UN12	50	3.07E-005	1627391	2458639.10	874.48	441.66	1172
2008 CM74	100	2.34E-005	4268663	2457264.83	1256.63	879.64	1780
2008 GM2	100	3.61E-005	2770077	2458975.81	1311.47	1171.95	3655
2008 HU4	100	3.00E-005	3328832	2457224.88	1035.92	753.40	1955
2008 JL24	25	4.84E-005	516288	2459949.27	1433.30	325.75	1363
2008 KT	100	2.97E-005	3365828	2456408.51	1782.00	630.00	1617
2008 LD	125	9.10E-005	1373068	2459989.80	1241.71	613.88	4829
2008 UA202	50	8.07E-005	619572	2460002.62	1169.51	216.58	1510
2008 UC202	150	4.63E-005	3242589	2460000.50	1743.97	1255.66	5019
2008 WO2	25	6.45E-005	387875	2456003.60	1601.62	593.86	3307
2009 BD	50	1.53E-005	3269580	2459426.64	1506.79	1145.79	1514
2009 WQ6	150	1.70E-004	880019	2457438.15	793.51	566.79	8347
2009 WW7	100	7.59E-005	1317322	2457444.81	1726.53	1430.06	9379
2009 WR52	100	3.43E-005	2911333	2456026.02	1674.21	1360.30	4037
2009 YR	100	2.22E-005	4511198	2458046.12	1495.43	807.53	1547
2010 JW34	100	2.71E-005	3692257	2456006.76	929.11	631.80	1478
2010 RF12	100	3.68E-005	2720770	2459962.67	1569.58	1083.01	3439
2010 UY7	100	4.57E-005	2187217	2456970.61	1485.00	1110.00	4385
2010 UE51	100	3.39E-005	2947759	2459989.98	574.26	511.09	1498
2010 VL65	100	3.96E-005	2525177	2458982.79	1395.18	1269.61	4344
2010 VQ98	100	2.91E-005	3436307	2456001.27	1454.87	419.96	1056
2011 AM37	25	5.70E-005	438624	2457412.01	1267.93	575.15	2832
2011 BQ50	100	3.54E-005	2828081	2459411.12	1073.59	694.04	2120
2011 CA7	25	1.36E-004	183947	2458886.58	947.17	393.77	4624
2011 CH22	125	1.04E-004	1200859	2456895.09	1220.78	964.42	8674
2011 JV10	25	5.83E-005	429034	2458969.75	1202.47	702.57	3537
2011 MD	100	2.44E-005	4095358	2460000.74	1381.23	878.96	1854
2011 UD21	50	2.15E-005	2324299	2456000.50	1214.02	637.67	1185
2012 AQ	50	4.59E-004	108966	2458872.57	348.79	136.03	5393
2012 EP10	25	2.76E-005	905924	2456000.75	1495.44	1181.40	2817
2012 FS35	25	1.30E-004	192527	2458399.34	824.95	254.76	2858

Table 9: Final results of the trajectory optimization considering the mass estimated using the upper limit of Method 2. For the 39 pruned asteroids ($H > 28$ and $0.85 <$semi-major axis< 1.15), we specify the Thrust (T), acceleration (a), departure epoch (DT), time of flight (TOF), the time where the thruster is on (T_{ON}) and the accumulated $\triangle V$ to perform the capture.

References

[1] Jet Propulsion Laboratory. Near Earth Observation Program. http://neo.jpl.nasa.gov/glossary/h.html, [Accessed on 5th of September 2012].

[2] H. Baoyin, Y. Chen and J. Li. Capturing Near Earth Objects. Research in Astronomy and Astrophysics 10(6) (2010) 587.

[3] D. Cohen, Earth's natural wealth: an audit. NewScientist, 23 May 2007.

[4] D.J. Scheeres, R.L. Schweickart., The mechanics of moving asteroids, Planetary Defense Conference: Protecting Earth from Asteroids, Orange County, CA, USA, February 23-26, 2004.

[5] J. Brophy, L. Friedman, and F. Culick, Asteroid Retrieval Feasibility Study. Keck Institute for Space Studies, Califonia Institute of Technology, Jet Propulsion Laboratory, 2012.

[6] C. Colombo, M. Vasile, G. Radice, Optimal low-thrust trajectories to asteroids through an algorithm based on differential dynamic programming. Celestial Mechanics and Dynamical Astronomy, 105(1-3) (2009) 75-112.

[7] K. Alemany, R.D. Braun, Survey of Global Optimization Methods for Low-Thrust, Multiple Asteroid Tour Missions. AAS/AIAA Space Flight Mechanics Meeting, Sedona, Arizona, USA, January 28 - February 1, 2007.

[8] J.T. Olympio, Optimal Control Problem for Low-Thrust Multiple Asteroid Tour Missions. Journal of Guidance, Control, and Dynamics 34(6) (2011) 1709-1720.

[9] B.W. Longmier, et al. VASIMR VX-200 Performance Measurements and Helicon Throttle Tables Using Argon and Krypton. 32nd International Electric Propulsion Conference, Weisbaden, Germany, September 11-15, 2011.

[10] J.P. Sanchez, C. Mcinnes., On the ballistic capture of asteroids for resource utilisation. 62nd International Astronautical Congress, Cape Town, South Africa, October 3-7, 2011.

[11] J.L. Hilton, Asteroid masses and densities. In Asteroids III (W. F. Bottke Jr. et al., eds.), this volume. Univ. of Arizona, Tucson, 2002

[12] S.R. Chesley, et al. Quantifying the Risk Posed by Potential Earth Impacts. Icarus 159 (2002) 423-432.

[13] J.W. Fowler and J.R. Chillemi. IRAS Minor Planet Survey 1992, ed. E.F. Tedesco, Phillips Laboratory Technical Report No. PL-TR-92-2049. Hanscom Air Force Base, MA, USA.

[14] J.P. Sanchez, D. Garcia Yarnoz and C.R. McInnes. Near-Earth Asteroid Resource Accessibility and Future Capture Mission Opportunities. Global Space Exploration Conference, Washington, DC, USA, May 22-24, 2012.

[15] J.A. Sims and S.N. Flanagan. Preliminary Design of Low-Thrust Interplanetary Missions. AAS 99-338, AAS/AIAA Astrodynamics Specialist Conference, Girdwood, Alaska, USA, August 16-19, 1999.

[16] G. Gómez, Á. Jorba, J.J. Masdemont, C. Simó, Dynamics and Mission Design Near Libration Points, Vol. III Advanced Methods for Collinear Points. World Scientific, 2001.

[17] R. Storn, K. Price, Differential evolution-a simple and efficient heuristic for global optimization over continuous spaces. Journal of global optimization 11(4) (1997) 341-359.

[18] C.H. Yam, D. di Lorenzo, D. Izzo, Low-Thrust Trajectory Design as a Constrained Global Optimization Problem. In Proceedings of the Institution of Mechanical Engineers, Part G: Journal of Aerospace Engineering, SAGE Publications, 225(11) (2011) 1243-1251.

[19] C.H. Yam, D. Izzo, F. Biscani, Towards a High Fidelity Direct Transcription Method for Optimisation of Low-Thrust Trajectories. 4th International Conference on Astrodynamics Tools and Techniques, Madrid, Spain, May 3-6, 2010.

[20] Y. Gao, Advances in low-thrust trajectory optimization and flight mechanics. PhD Thesis, University of Missouri-Columbia, 2003.

[21] P.E. Gill. User's Guide for SNOPT Version 7: Software for Large-Scale Nonlinear Programming. Department of Mathematics. University of California, San Diego, La Jolla, CA 92093-0112, USA.